Errors and uncertainties in simulation of steady, viscous flow past a circular cylinder at *Re* = 20 using a systematic approach

Aravind SEENI*,[1], Parvathy RAJENDRAN*,[1], Mamat HUSSIN[1], Farzad ISMAIL[1]

*Corresponding author
[1]School of Aerospace Engineering, Universiti Sains Malaysia,
Engineering Campus, Nibong Tebal, 14300 Penang, Malaysia,
aravind.seeni@student.usm.my*, aeparvathy@usm.my*, hussinm@usm.my,
aefarzad@usm.my

DOI: 10.13111/2066-8201.2020.12.3.17

Received: 14 January 2020/ Accepted: 15 July 2020/ Published: September 2020

Abstract: *The use of Computational Fluid Dynamics as a tool for design and analysis of aerospace systems is well established. Since the results generated by a CFD solver are numerical approximations, the solution is inherently produced with errors and uncertainties. In this paper, a simple fluid flow problem of laminar, incompressible flow past a circular cylinder at Reynolds number of 20 is allowed to be solved by the well-known finite-volume solver ANSYS Fluent. The effect of variations in mesh resolution, domain boundary location and residual criteria settings is investigated. For all the cases, finite, structured meshes of acceptable quality are used. The influence of variables on the cylinder's drag results is analyzed and discussed. An interesting pattern in results has been observed. The study on the variation in mesh resolution showed no presence of mesh independent solution. The study on the variation of the domain distance showed that it is necessary to increase the diameter of the circle several thousand times to obtain a domain independent solution.*

Key Words: *numerical errors, uncertainties, circular cylinder, grid independent solution, domain independent solution, drag coefficient*

1. INTRODUCTION

Computational Fluid Dynamics (CFD) is expected to continuously play an instrumental role in the design and analysis of aerospace systems and components [1]. It has become an important analysis and design tool, particularly in the field of aerodynamics. It is a known fact that results generated through CFD are not exact or true results of the problem. Rather, the results are numerical approximations to governing equations due to the presence of errors and uncertainties. According to AIAA Guide for the Verification and Validation of Computational Fluid Dynamics Simulations, an *error* is defined as "A recognizable deficiency in any phase or activity of modeling and simulation that is not due to lack of knowledge".

Similarly, *uncertainty* is defined as "A potential deficiency in any phase or activity of the modeling process that is due to the lack of knowledge" [2]. The errors in CFD are classified as follows: 1. Physical approximation error, 2. Round-off error, 3. Iterative convergence error, and 4. Discretization error. Physical approximation or modelling errors are concerned with formulating the model. This includes the errors in the partial differential equation describing

the flow and related to model simplification for CFD purpose to solve with a low computational expense. Round-off errors are defined as the errors that occur due to the floating point accuracy of digits of numbers being solved. This error can be mitigated by using double precision for solving instead of single precision for instance.

Iterative convergence errors can be defined as the errors that occur due to the incomplete convergence of the discrete system [3]. CFD codes use iterative methods by evaluating the difference between successive iterates and reducing the residual value to attain convergence. The residual value is allowed to reduce to zero or a convergence criterion of low order is set. This convergence criterion is important due to its significance in achieving a desired level of accuracy. An iterative approach is followed differently for a linear and non-linear system of equations. Its significance will be discussed in this paper.

Discretization error can be defined as the difference between the solution to the discretized equations and the original partial differential equation [3]. In other words, it is the difference between the numerical solution and the exact solution. The discretization process, which involves the conversion of differential equations into an algebraic system of equations, introduces errors. The discretization process introduces parameters such as element size and/or time step (Δt). It is referred to as truncation error for linear problems.

Discretization errors are assessed through an error estimate, error band or error bound during analysis or while performing validation studies. It also drives the grid adaptation processes in h-adaptation, r-adaptation and p-adaptation. The errors are generally estimated a-posteriori after estimation of the numerical solution.

Discretization errors are discussed with suitable examples in this paper. To estimate discretization errors, there are two types of error estimators, namely finite-element-based estimator and extrapolation-based error estimator. The Richardson extrapolation [4], [5] method can be used as an extrapolation-based error estimator to determine the relative error between numerical and exact solution, but only for a smooth linear problem with simple geometries. The Grid Convergence Index method [6] is another method which provides an "error band" as an error estimate.

In order to quantify errors in CFD, verification procedures have been developed to address the issue. Code verification and solution verification are two available procedures. In code verification, the reliability of the CFD code to perform simulation and provide results of high accuracy is tested. It can be related to software quality assurance. One approach to code verification is the Method of Manufactured Solutions. In solution verification, an assessment of errors in the numerical solution of a partial differential equation is performed. The code verification process supersedes the solution verification process.

This paper deals with error estimate due to different user-level settings which can be termed as a solution verification procedure. Here, error estimates are provided for iterative convergence error and discretization errors for a simple fluid dynamics problem. No error estimators discussed above will be used; rather, errors are listed and discussed subsequently.

2. FORMULATION OF THE FLUID FLOW PROBLEM

The problem of interest and consideration is a linear problem with simple geometry. The flow problem chosen is the steady, viscous, laminar, incompressible flow past a 2D circular cylinder. Flow past a circular cylinder is immensely investigated in the aerospace research community due to its applications in various structures such as rockets, missiles and projectiles. It is still gaining much interest, and some of the recent studies on flow past a circular cylinder are [7]–[14]. The flow past a circular cylinder has been subjected to intensive

research. A survey of studies that have investigated C_d for a circular cylinder at low Reynolds number (*Re*) will be performed. Only studies that considered steady, viscous, incompressible flow assumptions will be reviewed. Wieselsberger [15] studied the variation in C_d with an increase in fluid velocity for a cylinder and deduced that the opinion of Newton on the independency of C_d with fluid velocity is no longer applicable. It further states that the study by Lamb (1911) which specifies that C_d on a circular cylinder as a function of *Re* as $8\pi(Re(2.002 - \ln Re))^{-1}$ is derived from approximation theory and is applicable only for small cylinders with radius, $r = 1$. Similarly, as referenced in Hirota and Miyokoda [16], Imai (1957) proposes a similar functional relationship for C_d as $C_d = \left(0.707 + 3.42Re^{-1/2}\right)^2$.

Thom [17] proposed the arithmetic method to solve the equations of steady viscous flow and applied it to a finite circular cylinder. C_d values were proposed for varying *Re* based on calculations using the proposed arithmetic method. Kawaguti [18] performed a solution of flow past a two-dimensional (2D), viscous flow around a circular cylinder by solving numerically the exact Navier Stokes equations and found that the condition of steadiness holds true for *Re* of 40. The C_d values estimated in this work were found to be in good agreement with experimental data. Tritton [19] performed an experimental study in the analysis of flow past a circular cylinder for *Re* between 0.5 to 100. Here, as part of the study, measurements on drag were performed by observing the bending of quartz fibres and compared with other experimental and theoretical calculations. Apelt [20] also performed a numerical solution of the complete Navier Stokes equations in solving the flow past a circular cylinder at *Re* of 40.

The study also confirmed that a steady solution exists at the *Re* and a relatively less accurate steady solution was also obtained for *Re* of 44. Dennis and Shimshoni [21] studied the steady motion of a viscous, incompressible fluid past a circular cylinder for a range of *Re*. The calculated C_d was found to agree well with experimental result for *Re* up to 30, but variation was found to increase for higher *Re*. The results were compared with the calculations of Kawaguti [18] and Apelt [20].

In a further study, Kawaguti and Jain [22] performed a numerical study of viscous, incompressible flow past a circular cylinder and investigated the drag among other parameters for *Re* between 1 to 100. The study confirmed that the steady solutions exist for *Re* from 10 to 50, beyond which unsteady effects start. Underwood [23] studied the steady, viscous, incompressible flow past a circular cylinder for *Re* up to 10. The paper proposed a new method for accurately describing the flow field surrounding a circular cylinder using a semi-analytic method. The governing partial differential equations of motion were reduced to a system of ordinary differential equations and the flow field variables were determined. Among other parameters, the C_d results over the investigated *Re* range were estimated and validated with experimental results in this paper.

Dennis and Chang (1970) obtained the finite difference solutions of the equations of motion for steady, incompressible flow around a circular cylinder for *Re* range of 5 to 100. C_d, among other parameters were calculated for the range of *Re* and the results presented. A survey on newer research literature shows that the study on flow past a circular cylinder is still of major importance. Yousefifard et al. [8] compared the results obtained from structured and unstructured grids through numerical simulations of incompressible laminar flow over circular cylinder at *Re* range of ≤ 200 covering both steady and unsteady regime. Unstructured grid comprising triangular elements and structured grid comprising non-uniform rectangular elements were used. The numerically obtained results were validated with experimental results. Canuto and Taira [24] performed a 2D Direct Numerical Simulation (DNS) for studying compressible, viscous flow past a circular cylinder. The flow analysis was performed

by varying the *Re* between 20 and 100. The paper states that for *Re* from around 5 to 47, the separated flow behind the cylinder forms a steady, symmetric wake whereas beyond this critical *Re*, the flow becomes unsteady. Posdziech and Grundmann [25] investigated the flow on an infinitely long circular cylinder for *Re* between 5 and 250 using spectral element method. By assuming a laminar, incompressible flow, simulations were performed by varying the mesh resolution and size of computational domain. It was found that after increasing the size of the computational domain to several thousands of cylinder diameters, asymptotic solutions for drag coefficient were found. The drag coefficient was found to be strongly dependent on the mesh resolution size and more on the size of the computational domain. The results obtained successfully replicated experimental measurements accurately as opposed to the shortcomings of earlier approximations obtained numerically.

The above discussed studies are some of the studies related to current research. All studies have chosen a suitable scientific method for the study of flow past a circular cylinder. The following conclusions can be derived from henceforth. The C_d value depends on the *Re* and the freestream velocity of the flow. Secondly, the condition of the flow to be steady or unsteady also depends on the *Re* of the flow. For a circular cylinder, the transition from steady to unsteady lies around the critical *Re* of 47.

Correspondingly, in this work, a steady flow condition is assumed, and the *Re* selected for analysis is 20. Since the flow is steady, time-dependent simulations are not necessary and discrete simulations are consequently performed. In addition, viscous, incompressible flow around the cylinder will be assumed. The analysis will be performed using CFD for a cylinder with a radius of 1m. Only the drag coefficient (C_d) of the cylinder will be measured and discussed. The computational code considered for performing this analysis will be discussed in subsequent sections.

The objective of the paper is to investigate the errors and uncertainties of CFD usage concerning modelling and analysis of fluid flow problems. The focus of the study is the impact of various effects such as residual convergence criteria, grid size and domain size on result accuracy. Some interesting results have been obtained and will be subsequently discussed. Only discrete simulations are performed, as for the chosen Reynolds number, there will be no vortex shedding from the object. Only the variations in C_d are analyzed and discussed.

3. METHODOLOGY

Governing equations

The governing equations are the 2D incompressible Navier-Stokes equations. The flow is assumed to be laminar; hence there are no turbulence models included. The equations are expressed as follows [8].

$$\frac{\partial u}{\partial t} + u\frac{\partial u}{\partial x} + v\frac{\partial u}{\partial y} = -\frac{\partial p}{\partial x} + \frac{1}{Re}\left(\frac{\partial^2 u}{\partial x^2} + \frac{\partial^2 u}{\partial y^2}\right) \tag{1}$$

$$\frac{\partial v}{\partial t} + u\frac{\partial v}{\partial x} + v\frac{\partial v}{\partial y} = -\frac{\partial p}{\partial x} + \frac{1}{Re}\left(\frac{\partial^2 v}{\partial x^2} + \frac{\partial^2 v}{\partial y^2}\right) \tag{2}$$

$$\frac{\partial u}{\partial x} + \frac{\partial v}{\partial y} = 0 \tag{3}$$

where p is the pressure, ρ is the density, *Re* is the Reynolds number given by the following form: $Re = \frac{\rho U d}{\mu}$ depends on the density, velocity of freestream flow U, diameter of circular cylinder d, and the dynamic viscosity of fluid μ.

Code selection

There are several computational codes available to solve the discrete Navier-Stokes equations of incompressible flow. Among the available options, the finite volume solver ANSYS Fluent v16.0 is chosen as the preferred computational code due to the reason that it has been successfully implemented in several scientific studies encompassing diverse fields such as nuclear engineering, chemical engineering, mechanical engineering, energy etc. [26]–[32]. The capability of the selected code to achieving high result accuracy is of primary importance in the present work and has been verified from the literature [33]–[36].

Mesh

For analyzing the case of estimating the errors associated with grid sizing, different grids of an increasing number of elements are designed. The meshes are modelled in ANSYS [37]. Meshes must be designed with high quality cells to produce highly accurate solutions as well as ensuring numerically stability. Quadrilateral elements are used to maintain a high degree of mesh quality. The quality of a cell in a mesh or the mesh itself is defined based on the parameters, namely, orthogonality, skewness and aspect ratio. Orthogonality or orthogonal quality of a cell is computed using the vector from the centroid of the cell to each of cell's faces, face area vector and vector from centroid of the cell to the centroid of the adjacent cells [38]. This is illustrated in Fig. 1. A low value close to 0 indicates a cell of low quality, whereas a value close to 1 indicates a cell of high quality. The minimum orthogonal quality, used here, therefore, describes a mesh with the lowest cell value.

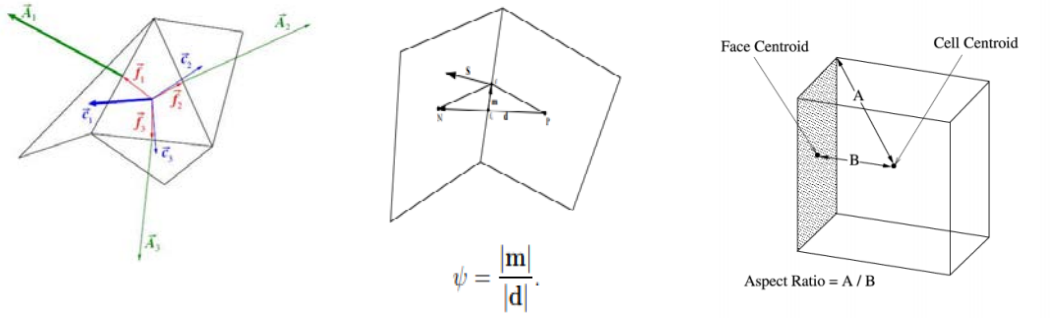

$$\psi = \frac{|\mathbf{m}|}{|\mathbf{d}|}.$$

(a) (b) (c)

Fig. 1 – Illustrative description of mesh quality parameters (a) Orthogonal quality [38] (b) Skewness [39] and (c) Aspect ratio [38]

In total, 9 grids are designed, M1 to M9, as detailed in Table 1. Meshes M1, M2 and M3, have a minimum orthogonal quality close to 1, while other meshes have a minimum orthogonal quality of exactly 1. Skewness can be defined as the difference between the shape of a cell and the shape of an equilateral cell which has equivalent volume [38]. High skewness is an undesirable parameter because it reduces accuracy and causes destabilization of solution. An optimal skewness in a quadrilateral mesh must be at least less than 0.95 and significantly lower than that value with vertex angles close to 90^0. The definition is further provided in the form illustrated in Fig. 1.

The maximum orthogonal skewness decreases with increasing mesh resolution, which indicates increasing quality. Aspect ratio defines the degree of stretching imparted to cell [38]. The definition of aspect ratio is illustrated in Fig. 1.

An O-grid topology is employed that includes structured mesh. In all the grids, the diameter of the cross-section of the cylinder (i.e. circle) is fixed with a diameter (d) of 1m. The 9 grids, M1 to M9 are pictorially represented in Fig. 2. The grids consist of increasing the

resolution from one mesh to the other, such that the radial divisions are doubled for each increasing mesh sizing.

The circumferential and radial divisions are maintained in such a way, that the increase in mesh size improves the overall mesh quality from M1 to M9, as illustrated in Table 1. A constant domain size of 64d is maintained across all these grids.

For estimating the errors due to domain sizing, grids of increasing domain size are designed. The grids consist of increasing the diameter of domain around the circular cylinder, under uniformity from 32d to 512d, as illustrated in Fig. 3. Also, in this case, like the previous case of studying errors associated with grid sizing, quadrilateral elements are used to maintain a high degree of accuracy.

The radial and circumferential divisions are maintained under uniformity across the grids, M10 to M14 in such a way that a constant grid resolution is maintained as illustrated in Table 2. A constant grid size of 192×96 is maintained across these grids. This size is chosen based on the study on the effect of grid size (to be discussed later).

Table 1 – Grid refinements used to study discretization errors (of mesh size) along with grid quality parameters

No.	Grid	Cells	Faces	Nodes	Min. orthogonal quality	Max. orthogonal Skew	Max. aspect ratio
M1	24 x 12	288	600	312	0.992	8.29E-03	4.91
M2	48 x 24	1152	2352	1200	0.998	2.06E-03	4.35
M3	96 x 48	4608	9312	4704	0.999	5.13E-04	4.10
M4	192 x 96	18432	37056	18624	1.00	1.28E-04	3.98
M5	384 x 192	73728	147840	74112	1.00	3.19E-05	3.92
M6	576 x 288	165888	332352	166464	1.00	1.42E-05	3.90
M7	768 x 384	294912	590592	295680	1.00	7.98E-06	3.89
M8	960 x 480	460800	922560	461760	1.00	5.10E-06	3.89
M9	1152 x 576	663552	1328256	664704	1.00	3.54E-06	3.88

Table 2 – Grid refinements used to study errors due to domain size variation

No.	Domain size	Cells	Faces	Nodes	Total mesh volume (m^3)	Min. orthogonal quality	Max. orthogonal skew	Max. aspect ratio
M10	32d	18432	37056	18624	8.03E+02	1.00	1.29E-04	4.50
M11	64d	18432	37056	18624	3.22E+03	1.00	1.28E-04	3.98
M12	128d	18432	37056	18624	1.29E+04	1.00	1.26E-04	3.60
M13	256d	18432	37056	18624	5.15E+04	1.00	1.25E-04	3.30
M14	512d	18432	37056	18624	2.06E+05	1.00	2.31E-04	3.05

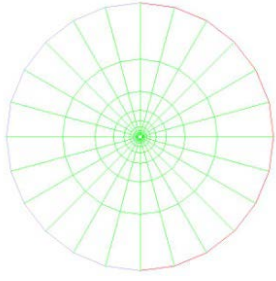

(a) M1: 64d, 24×12

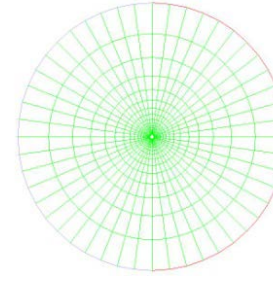

(b) M2: 64d, 48×24

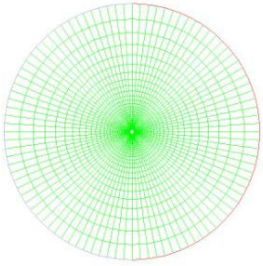

(c) M3: 64d, 96×48

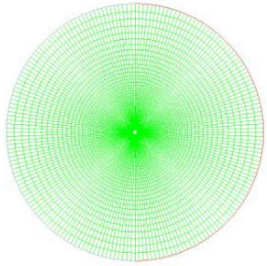

(d) M4: 64d, 192×96

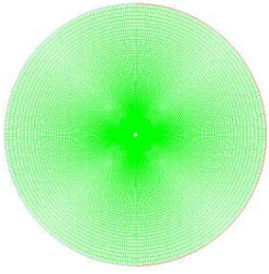

(e) M5: 64d, 384×192

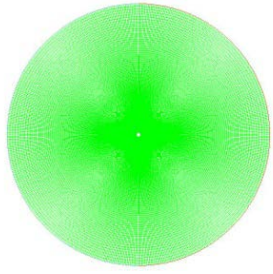

(f) M6: 64d, 576×288

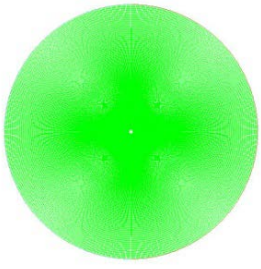

(g) M7: 64d, 768×384

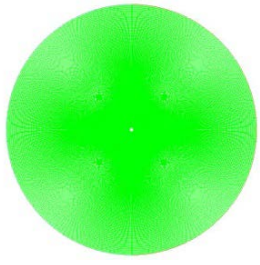

(h) M8: 64d, 960×480

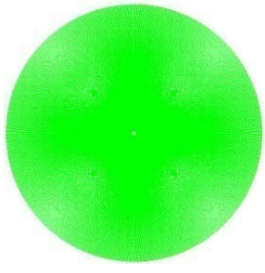

(i) M9: 64d, 1152×576

Fig. 2 – Grids with uniformly increasing mesh resolution, M1 to M9

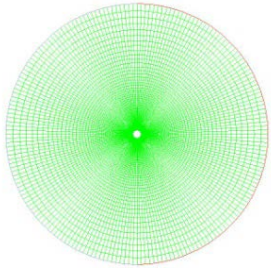

(a) M10: 32d, 192×96

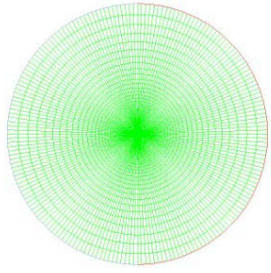

(b) M14: 512d, 192×96

Fig. 3 – Grids with different domain size, M10 and M14, under uniformity of total cell number or grid size

Boundary conditions

The flow is assumed to be viscous, laminar. The *Re* of the flow is set as 20. For this *Re* case, the flow regime is steady and dealt with accordingly. The fluid is assumed to have a density of $1kg/m^3$ with a viscosity of $0.05kgm^{-1}s^{-1}$. The inlet is specified with the flow velocity of 1m/s. A no-slip shear condition is imposed on the cylinder wall. The outlet is specified with a pressure of 0Pa. The boundary conditions are also illustrated in Fig. 4.

Solution scheme

A pressure-based solver is assumed in ANSYS to solve the governing equations. The Semi-Implicit Pressure Linked Equations (SIMPLE) scheme is chosen for pressure-velocity coupling. The SIMPLE algorithm uses a relationship between velocity and pressure corrections for enforcing mass conservation to estimate the pressure field [40]. A least-squares cell based algorithm is assumed for gradients. The pressure and momentum are assigned with a second-order interpolation scheme for improved accuracy. The computations were performed in a workstation powered by a 2.5GHz Quadcore processor and supported by 8GB RAM.

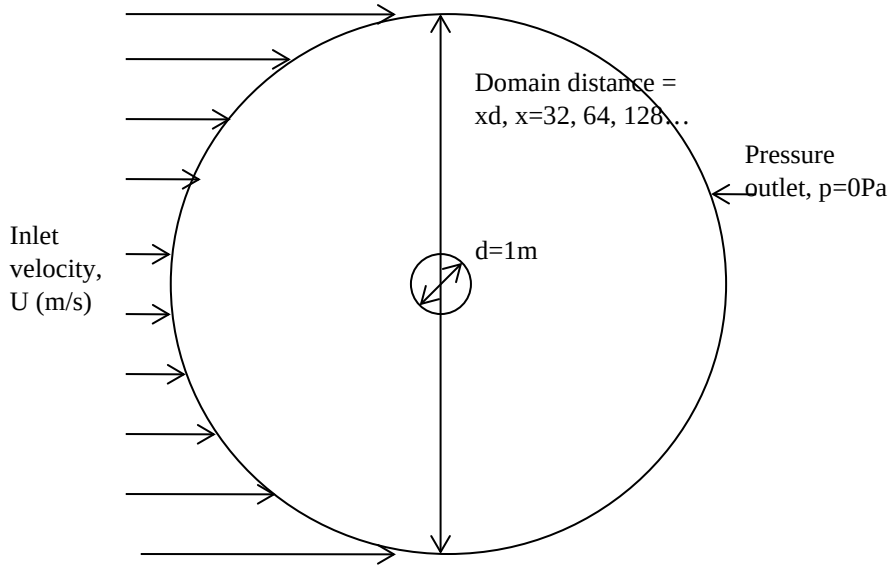

Fig. 4 – Description of imposed boundary conditions in the computational domain

Expressions for pressure drag, viscous drag and total drag coefficients

The drag force in the case of a streamlined body such an airfoil is the horizontal component of the resultant force exerted by the fluid on the body, whereas for a symmetric body such as a cylinder, the resultant force exerted by the fluid on the entire surface of the cylinder forms the drag. The total drag is composed of two components, which are skin friction drag caused by shearing force and pressure drag. In low *Re* viscous flows, the pressure drag forms the majority of total drag, whereas viscous drag is relatively small. This total drag can be expressed as,

$$D_t = D_p + D_f \tag{4}$$

where D_t is the total drag, D_p is the pressure drag, and D_f is the friction drag. The total drag can also be expressed using notations representing a circle by the following relationship [16],

$$D_t = -\int_0^{2\pi} P_0 \cos\theta \, d\theta - \rho v \int_0^{2\pi} \zeta_0 \sin\theta d\theta \tag{5}$$

where P_0 is the static pressure, ζ_0 is the vorticity on the surface of the cylinder, and θ is the angle between the central axis to the point on the surface of the cylinder. The total drag coefficient, C_d is used to express the non-dimensionalized form of drag force (D) as,

$$C_d = \frac{D}{0.5\rho V^2 S} \tag{6}$$

where S is the cross-sectional area of the cylinder, the non-dimensional form of D is estimated numerically in the present work, and the pressure ($C_{d,p}$) and skin-friction ($C_{d,f}$) drag component results are presented separately.

4. RESULTS AND DISCUSSIONS

Benchmark solution for C_d at Re=20

In the paper, as referenced by Canuto and Taira [24], Tritton [19] suggested that C_d for circular cylinder present in a flow of Re=20 is 2.09. Similarly, as in Canuto and Taira [24], Linnick and Fasel [41] suggested C_d for Re=20 as 2.06. The study by Taira and Colonius [42] also proposed C_d for the same flow condition as 2.06. Dennis and Chang [43] obtained finite difference solutions of the equations of motion for steady, incompressible past a circular cylinder for Re range from 5 to 100. The C_d for Re=20, according to this study, was suggested as 2.05, as in Taira and Colonius [42].

The values proposed by Fornberg [44] is used as a benchmark result for C_d in the present study due to the following reasons as in Table 3. The C_d values proposed by Tritton [19] appears to be slightly over-estimated outright, as found in comparison to other studies. Linnick and Fasel [41] used a modified boundary interface method for the discretization of Navier Stokes equations to perform their numerical computations as also in the study by Taira and Colonius [42]. In the study by Linnick and Fasel [41], two spatial domain discretization was employed, and the study proposed non-identical C_d results as a final solution.

Table 3 – Comparison of past studies on *Cd* of a circular cylinder for *Re*=20

No.	Study	C_d for Re=20
1	Tritton [19]	2.09
2	Linnick and Fasel [41]	2.06
3	Dennis and Chang [43]	2.05
4	Taira and Colonius [42]	2.06
5	Fornberg [44]	2.0001±0.0002

Fornberg [44] in his paper proposed a numerical method to study the flow past a circular cylinder by assuming a steady, viscous, incompressible flow. The Re of flow investigated is from 20 to 300. The computations were performed in a computer CDC STAR 100 with an average computational speed of 16 Mflops/sec. The C_d values were computed by varying the radius (r) of a cylinder for 3 cases namely coarse grid, fine grid and Richardson extrapolation. The differences between these curves gave the C_d values that are independent of r. The value of C_d for Re=20 (Fig. 5) is suggested with an error band as,

$$C_d = 2.0001 \pm 0.0002 \tag{7}$$

This result will be treated as a benchmark solution in the present study.

Effect of residual criteria setting

The effect on the results of $C_{d,p}$, $C_{d,f}$ and $C_{d,t}$ with variation in residual criteria setting is first investigated.

A grid size of 192×96 is chosen. The residual criteria are varied between 1e-3 to 1e-9 in uniformly decreasing order of 1e-1. The computed results of the various drag coefficients, number of iterations recorded for attaining convergence and the total computational time are listed in Table 4.

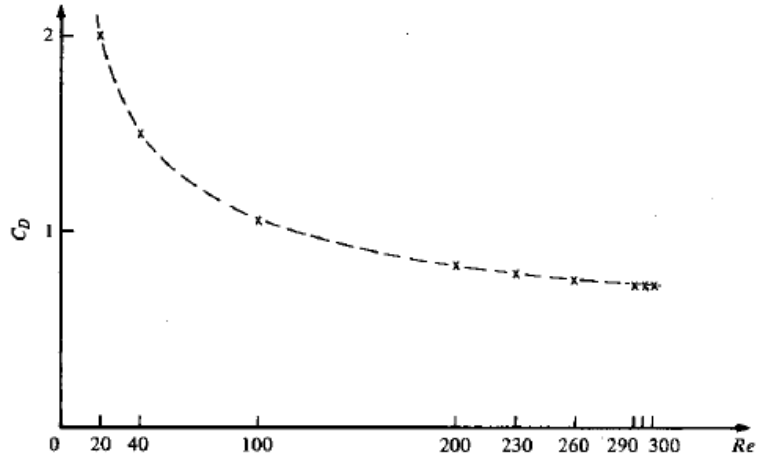

Fig. 5 – Fornberg's C_d as a function of *Re*. For *Re* of 20 investigated, the C_d estimate is 2.0001±0.0002 [44].

Table 4 – Effect of residual criteria setting on pressure, viscous, total drag coefficient and computational cost

Set residual criteria	$C_{d,p}$	$C_{d,f}$	$C_{d,t}$	No. of iterations	Total computational time (s)
1.00E-03	1.179374	2.058788	3.238162	82	1.68
1.00E-04	1.229090	0.850795	2.079885	659	11.604
1.00E-05	1.225220	0.818978	2.044198	1119	19.388
1.00E-06	1.224818	0.815887	2.040705	1576	28.718
1.00E-07	1.224777	0.815582	2.040359	2031	36.512
1.00E-08	1.224773	0.815551	2.040324	2486	41.637
1.00E-09	1.224773	0.815548	2.040321	2950	48.997

The relative error between $C_{d,t}$ obtained in the present study and benchmark results of Fornberg [44] are then estimated using the following formula.

$$\Delta C_d(\%) = \left| \frac{C_{d,t} - C_{d_{bm}}}{C_{d_{bm}}} \right| \times 100 \tag{8}$$

where ΔC_d is the iterative convergence error, $C_{d,t}$ is the total drag coefficient, and C_{dbm} is the benchmark drag coefficient.

The error results are estimated using Eqn. 8 and provided in Table 5. It can be found that the least error of 2% is provided by the criteria setting of 1e-06 and lower.

A compromise between result accuracy and computational expense needs to be determined.

Hence the residual criterion of 1e-06 is sufficient and found to have achieved a reasonable level of accuracy in our simulations.

Criteria set above 1e-06 are not sufficient as the level of accuracy achieved by the residuals is not small enough to attain convergence.

Table 5 – Error percentage of $C_{d,t}$ due to residual criteria setting

Residual criteria	Error (%)
1.00E-03	61.9
1.00E-04	4.0
1.00E-05	2.2
1.00E-06	2.0
1.00E-07	2.0
1.00E-08	2.0
1.00E-09	2.0

Effect of mesh resolution

The error due to variation in mesh size (Δx, Δy) is an important source of error called the discretization error or truncation error for linear problems. To study its impact, simulations are performed for uniformly varying mesh sizes as detailed in Table 6 by assuming a residual criterion of 1e-06. This residual criterion is set based on the original finding that a minimum residual criterion of convergence set does not increase the error any further. The domain geometry is set with a diameter of 64d. Table 6 details the variation in C_d estimation due to mesh size variations.

Table 6 – Effect of mesh resolution variation on pressure, viscous, total drag coefficient

Case	Mesh size	$C_{d,p}$	$C_{d,f}$	$C_{d,t}$
Case 1	24 x 12	1.244850	0.845127	2.089977
Case 2	48 x 24	1.218757	0.828599	2.047356
Case 3	96 x 48	1.220402	0.820216	2.040618
Case 4	192 x 96	1.224818	0.815887	2.040705
Case 5	384 x 192	1.228201	0.816910	2.045111
Case 6	576 x 288	1.230777	0.828591	2.059369
Case 7	768 x 384	1.233933	0.851761	2.085694
Case 8	960 x 480	1.236835	0.879377	2.116212
Case 9	1152 x 576	1.239080	0.907351	2.146431

Table 7 lists the error due to discretization by comparing that was evaluated using Eqn. 8 for different cases of mesh sizes. For structured mesh of uniform grid refinements, the C_d results typically lie in asymptotic range. However, in our case, an interesting result has been obtained in which the C_d error stabilizes at 2% and then the error increases to 2.3% with further mesh resolution increase before accumulating more errors with increasing refinements.

Table 7 – Error percentage of *Cd,t* due to mesh resolution variation

Case	Mesh size	Error (%)
Case 1	24 x 12	4.5
Case 2	48 x 24	2.4
Case 3	96 x 48	2.0
Case 4	192 x 96	2.0
Case 5	384 x 192	2.3
Case 6	576 x 288	3.0
Case 7	768 x 384	4.3
Case 8	960 x 480	5.8
Case 9	1152 x 576	7.3

The above mentioned procedure to determine the C_d for increasing the mesh resolution is followed to compute the mesh independent solution. Based on the discussion of estimated errors, it can, therefore, be stated that a mesh independent result could not be clearly identified. Despite the usage of high mesh quality and well validated software code, a mesh independent solution does not exist. Further scrutiny of this source of uncertainty is therefore required.

Effect of computational domain size

The error due to the variation in computational domain size is also studied as they are also a source of error. 5 grids, M10 to M14 as listed in Table 2 are simulated. The effect of outer boundary location is studied by keeping the diameter of cylinder cross-section constant and varying the domain size by doubling the distance in steps as such, 32d, 64d, 128d, 256d, 512d. The mesh sizing of 192x96 that was suggestive of the previous result is kept constant throughout. Also, the residual error is set at 1e-06 for convergence. Table 8 summarizes the results obtained through the simulations conducted, as per the settings discussed.

Table 8 – Effect of computational domain size on pressure, viscous, total drag coefficient and computational cost

Domain size	$C_{d,p}$	$C_{d,f}$	$C_{d,t}$	No. of iterations	Total computational time (s)
32d	1.262388	0.835548	2.097936	1685	28.136
64d	1.224818	0.815887	2.040705	1576	25.846
128d	1.208817	0.807943	2.016759	1481	25.766
256d	1.201482	0.804737	2.006218	1401	25.562
512d	1.197764	0.803512	2.001276	1339	25.599

For the variable domain size, it was found that as the distance to outer boundary increases from 32d to 512d, for mesh M10 to M14, the values of C_d increase in accuracy and approach the benchmark values. Also, it was found that the number of iterations required for convergence decreases gradually when computing from 32d to 512d. The number of iterations required for 32d is about 1685 compared to 1339 iterations for the larger boundary distance of 512d. Despite the decreasing number of iterations, the computational time required to perform the iterations do not vary significantly. The time for computing the 32d grid is about 28.1s compared to approximately 25 seconds for the other grids.

The error due to the increase in boundary location is calculated using Eqn. 4 and summarized in Table 9. It was shown that the relative error between grids M10 to M14 and benchmark values decrease gradually to almost zero. Hence it can be said that a domain size of 512d is more accurate, although other grids provided results in the acceptable error range of ±10%. The above described procedure of increasing the boundary location or domain size is to compute the domain independent solution of C_d.

Table 9 – Error percentage of *Cd,t* due to computational domain size variation

Domain size	Error (%)
32d	4.9
64d	2.0
128d	0.8
256d	0.3
512d	0.1

Domain independence is also essential to the problem due to discretization errors. It can be found that increase in domain size up to 512d has reduced the relative error to 0.1% and a further increase of this size may ultimately lead to an even lower error. However, due to

limitations in software code, the maximum domain size that could be achieved in the present configuration is 999d, beyond which the code's limitation restricts further investigation of domain size. However, in another study by Posdziech and Grundmann [25], the domain increase has been investigated to several thousands of diameter until asymptotic solutions of C_d has been found. The difference between the current research and that of Posdziech and Grundmann [25] is the increased accuracy of C_d estimate relative to experimental measurements. Due to limitations in software code, in the present study, this could not be investigated, and additional studies still need to be performed.

Effect of Reynolds number

So far, the effect of variation in residual criteria, discretization and domain size have been studied and the error patterns analyzed and discussed. The Reynolds number for all these cases has been fixed at 20. The effect of *Re* on C_d is not so far investigated. Simulations are conducted for flow *Re* of 50, 100 and 500. The mesh grid assumed is M4 with grid dimensions of 192x96. The domain size is assumed as 64d. The residual criteria for convergence are set at 1e-6 based on the earlier result. The results are compared with experimental results of Fornberg [44] for *Re* 50 and 100. For *Re* of 500, experimental results are not available. The computed results are provided in Table 10.

Table 10 – Effect of Reynolds number on pressure, viscous, total drag coefficient

Re	$C_{d,p}$	$C_{d,f}$	$C_{d,f}/C_{d,p}$	$C_{d,t}$	$C_{d,bm}$ [44]	Error (%)
50	0.9397	0.4579	0.4872	1.3976	1.3827	1.1
100	0.7937	0.2897	0.3651	1.0834	1.0612	2.1
500	0.7093	0.1147	0.1617	0.8241	-	-

As expected, the numerical result showed a gradual decrease in drag with the increase in Re. The ratio of frictional drag coefficient to pressure drag coefficient, $C_{d,f}/C_{d,p}$ also showed a gradual decrease. When the $C_{d,t}$ values are compared with benchmark values, the numerical results displayed minimal error. The numerical error computations are found within an acceptable range of < 5%, thus validating obtained results.

5. CONCLUSIONS

In this paper, a simple fluid flow problem of laminar, incompressible flow past a circular cylinder at low *Re* is assumed for performing computational studies. Studies were conducted to estimate the iterative convergence and discretization errors in the system. The spatial domain consisted of meshes of varied resolution as well as domain boundary size. In total, 14 meshes with structured discretization were employed to study discretization errors. The total drag coefficient of the cylinder is computed and used as the parameter for discussion in this work. Comparisons on drag data available from literature are performed to estimate the relative errors. The study on iterative convergence was performed by studying the effect of variation in residual criterion setting from 1e-3 to 1e-9. It was found that a 1e-6 residual criterion provides the best results with regards to accuracy and computational cost. The study on discretization error due to variation in mesh resolution showed that there is no mesh independent solution. The study on discretization error due to variation in domain boundary size showed the limitations of the computational code used in the present study. Although a very low relative error of 0.1% was obtained from the simulations, a further increase in domain size was still required to obtain domain independent results. Due to limitations in the code, this study could only be performed for a maximum acceptable domain size of 512 diameters.

It was found that only an increase in the size of diameters to thousands could provide the desired result. Future research could address the effect of high *Re* flows, errors and uncertainties due to flow unsteadiness and the usage of CFD turbulence models.

REFERENCES

[1] P. R. Spalart and V. Venkatakrishnan, On the role and challenges of CFD in the aerospace industry, *Aeronaut. J.*, vol. **120**, no. 1223, pp. 209–232, 2016.

[2] * * * AIAA, Guide for the verification and Validation of Computational Fluid Dynamics Simulations, *AIAA Standard G-077-1998*, 1998.

[3] C. J. Roy, Review of code and solution verification procedures for computational simulation, *J. Comput. Phys.*, vol. **205**, pp. 131–156, 2005.

[4] L. Richardson, The Approximate Arithmetical Solution by Finite Differences of Physical Prohlems involving Differential Equations, with an Application to the Stresses in a Masonry Dam, *Philos. Trans. R. Soc. London. Ser. A, Contain. Pap. a Math. or Phys. Character*, vol. **210**, pp. 307–357, 1910.

[5] L. Richardson and J. Gaunt, The Deferred Approach to the Limit Part I. Single Lattice. Part II. Interpenetrating Lattices, *Philos. Trans. R. Soc. London. Ser. A, Contain. Pap. a Math. or Phys. Character*, vol. **CCXXV**I, pp. 299–361, 1927.

[6] P. J. Roache, Perspective: A Method for Uniform Reporting of Grid Refinement Studies, *J. Fluids Eng.*, vol. **116**, pp. 405–413, 1994.

[7] B. N. Rajani, A. Kandasamy and S. Majumdar, On the Reliability of Eddy Viscosity Based Turbulence Models in Predicting Turbulent Flow past a Circular Cylinder Using URANS Approach, *J. Appl. Fluid Mech.*, vol. **5**, no. 1, pp. 67–79, 2012.

[8] M. Yousefifard, P. Ghadimi and R. Zamanian, Unstructured Grid Solutions for Incompressible Laminar Flow over a Circular Cylinder Using a Particular Finite Volume-Finite Element Method, *J. Eng.*, vol. **2013**, pp. 1–9, 2013.

[9] B. Apacoglu, A. Paksoy and S. Aradag, CFD Analysis and Reduced Order Modeling of Uncontrolled and Controlled Laminar Flow Over a Circular Cylinder, *Eng. Appl. Comput. Fluid Mech.*, vol. **5**, no. 1, pp. 67–82, 2014.

[10] X. Liu, A. Wei, K. Luo and J. Fan, Numerical study of the effects of particles on the near wake around a circular cylinder, *Int. J. Comut. Fluid Dyn.*, vol. **29**, no. 2, pp. 150–160, 2015.

[11] B. N. Rajani, A. Kandasamy and S. Majumdar, LES of Flow past Circular Cylinder at *Re* = 3900, *J. Appl. Fluid Mech.*, vol. **9**, no. 3, pp. 1421–1435, 2016.

[12] G. F. Smaisim, M. O. Fatla, A. Valera-Medina, A. M. Rageb and N. Syred, Experimental and theoretical investigation of the effect of rotating circular cylinder speed on the lift and drag forces, *Int. J. Energy Environ.*, vol. **7**, no. 1, pp. 23–36, 2016.

[13] R. Deepakkumar, S. Jayavel and S. Tiwari, Cross Flow past Circular Cylinder with Waviness in Confining Walls near the Cylinder, *J. Appl. Fluid Mech.*, vol. **10**, no. 1, pp. 183–197, 2017.

[14] J. Gou, X. Su and X. Yuan, Adaptive mesh refinement method-based large eddy simulation for the flow over circular cylinder at *Re* D = 3900, *Int. J. Comut. Fluid Dyn.*, vol. **32**, no. 1, pp. 1–18, 2018.

[15] C. Wieselsberger, New Data on the Laws of Fluid Resistance, *Phys. Zeitschrift*, vol. **22**, pp. 1–15, 1921.

[16] I. Hirota and K. Miyakoda, Numerical Solution of Karman Vortex Sheet behind a Circular Cylinder, *J. Meteorol. Soc. Japan*, vol. **43**, no. 1, pp. 30–41, 1964.

[17] A. Thom, Flow Past Circular Cylinders at Low Speeds, *Proc. R. Soc. London . Ser. A , Contain. Pap. a Publ. by R. Soc.*, vol. **141**, pp. 651–669, 1933.

[18] M. Kawaguti, Numerical Solution of the Navier-Stokes Equations for the Flow around a Circular Cylinder at Reynolds Number 40, *J. Phys. Soc. Japan*, vol. **8**, no. 6, pp. 747–757, 1953.

[19] D. J. Tritton, Experiments on the flow past a circular cylinder at low Reynolds numbers, *J. Fluid Mech.*, vol. **6**, no. 4, pp. 4–8, 1959.

[20] C. J. Apelt, The Steady Flow of a Viscous Fluid Past a Circular Cylinder at Reynolds Numbers 40 and 44, *Aeronautical Research Council Reports and Memoranda*, London, 1961.

[21] S. C. R. Dennis and M. Shimshoni, The Steady Flow of a Viscous Fluid past a Circular Cylinder, *Aeronaut. Res. Counc. Curr. Pap.*, vol. **797**, 1964.

[22] M. Kawaguti and P. Jain, Numerical Study of a Viscous Fluid Flow past a Circular Cylinder, *J. Phys. Soc. Japan*, vol. **21**, no. 10, pp. 2055–2062, 1966.

[23] R. L. Underwood, Calculation of incompressible flow past a circular cylinder at moderate Reynolds numbers, *J. Fluid Mech.*, vol. **37**, no. 1, pp. 95–114, 1969.

[24] D. Canuto and K. Taira, Two-dimensional compressible viscous flow around a circular cylinder, *J. Fluid Mech.*, vol. **785**, pp. 349–371, 2015.
[25] O. Posdziech and R. Grundmann, A systematic approach to the numerical calculation of fundamental quantities of the two-dimensional flow over a circular cylinder, *J. Fluids Struct.*, vol. **23**, no. 3, pp. 479–499, 2007.
[26] K. Gosiewski and A. Pawlaczyk-Kurek, Aerodynamic CFD simulations of experimental and industrial thermal flow reversal reactors, *Chem. Eng. J.*, vol. **373**, pp. 1367–1379, 2019.
[27] M. Khan, N. Zhao and T. Xu, Assessment of PECM as an efficient numerical analysis tool for investigating convective heat transfer phenomena during PCM melting, *J. Energy Storage*, vol. **24**, 2019.
[28] I. Razgallah, S. Kaidi, H. Smaoui and P. Sergent, The impact of free surface modelling on hydrodynamic forces for ship navigating in inland waterways: water depth, drift angle, and ship speed effect, *J. Mar. Sci. Technol.*, vol. **24**, no. 2, pp. 620–641, 2019.
[29] S. M. Seyyedi, A. S. Dogonchi, M. Hashemi-Tilehnoee, Z. Asghar, M. Waqas and D. D. Ganji, A computational framework for natural convective hydromagnetic flow via inclined cavity: An analysis subjected to entropy generation, *J. Mol. Liq.*, vol. **287**, 2019.
[30] T. Rämä, T. Toppila, D. C. Visser and N. B. Siccama, Validation of ice condenser model for CFD analysis of VVER-440 type containment, *Nucl. Eng. Des.*, vol. **352**, 2019.
[31] H. Choi and J. Cho, Aerodynamic Analysis and Parametric Study of the Blended-Wing-Body-Type Business Jet, *Int. J. Aeronaut. Sp. Sci.*, vol. **20**, no. 2, pp. 335–345, 2019.
[32] I. Gallego-Marcos *et al.*, Pool stratification and mixing induced by steam injection through spargers: CFD modelling of the PPOOLEX and PANDA experiments, *Nucl. Eng. Des.*, vol. **347**, pp. 67–85, 2019.
[33] A. Goltsman and I. Saushin, Flow pattern of double-cavity flow at high Reynolds number, *Phys. Fluids*, vol. **31**, no. 6, 2019.
[34] X. B. Chen, H. P. Lee, V. F. H. Chong and Y. De Wang, Assessment of septal deviation effects on nasal air flow: A computational fluid dynamics model, *Laryngoscope*, vol. **119**, no. 9, pp. 1730–1736, 2009.
[35] B. Blocken, T. Stathopoulos and J. Carmeliet, CFD simulation of the atmospheric boundary layer: wall function problems, *Atmos. Environ.*, vol. **41**, no. 2, pp. 238–252, 2007.
[36] R. Gupta, D. F. Fletcher and B. S. Haynes, On the CFD modelling of Taylor flow in microchannels, *Chem. Eng. Sci.*, vol. **64**, no. 12, pp. 2941–2950, 2009.
[37] J. Singleton and R. Baskaran, *FLUENT - Steady Flow Past a Cylinder*, Cornell University (Online), 2019. [Online]. Available: https://confluence.cornell.edu/display/SIMULATION/FLUENT+-+Steady+Flow+Past+a+Cylinder. [Accessed: 15-Jun-2019].
[38] * * * ANSYS Inc., *ANSYS FLUENT User's Guide*, Canonsburg, PA, USA, 2010.
[39] F. Juretic, *Error Analysis in Finite Volume CFD*, Imperial College London, 2004.
[40] * * * ANSYS Inc., *ANSYS FLUENT Theory Guide*, Canonsburg, PA, USA, 2013.
[41] M. N. Linnick and H. F. Fasel, A high-order immersed interface method for simulating unsteady incompressible flows on irregular domains, *J. Comput. Phys.*, vol. **204**, no. 1, pp. 157–192, 2005.
[42] K. Taira and T. Colonius, The immersed boundary method: A projection approach, *J. Comput. Phys.*, vol. **225**, no. 2, pp. 2118–2137, 2007.
[43] S. C. R. Dennis and G.-Z. Chang, Numerical solutions for steady flow past a circular cylinder at Reynolds numbers up to 100, *J. Fluid Mech.*, vol. **42**, no. 3, pp. 471–489, 1970.
[44] B. Fornberg, A numerical study of steady viscous flow past a circular cylinder, *J. Fluid Mech.*, vol. **98**, no. 4, pp. 819–855, 1980.